crystals

MDPI

Article

Mechanical Properties of Low Carbon Alloy Steel with Consideration of Prior Fatigue and Plastic Damages

Qing Liu [1], Zhanzhan Tang [1,*], Xuan Yang [1], Zhixiang He [1], Hanyang Xue [1] and Hanqing Zhuge [2]

[1] College of Civil Science and Engineering, Yangzhou University, Yangzhou 225127, China; mz120211015@stu.yzu.edu.cn (Q.L.); mz120210974@stu.yzu.edu.cn (X.Y.); mz120190743@yzu.edu.cn (Z.H.); dx120200087@yzu.edu.cn (H.X.)

[2] College of Civil Engineering and Architecture, Zhejiang University of Science & Technology, Hangzhou 310023, China; 120043@zust.edu.cn

* Correspondence: tangzhanzhan@126.com

Abstract: Mechanical properties, including the fatigue behavior of metals, are usually determined from damage-free specimens, but it is not well known how these properties change with respect to prior damages; hence, the present work aims to understand the remaining mechanical properties of low carbon alloy steel Q345q with pre-damages. Low-cycle fatigue tests on the damage free specimens, tensile tests on the low-cycle fatigue damaged specimens, and fatigue tests on the plastic deformed specimens were carried out, respectively. The low-cycle fatigue life prediction formula was proposed. The influences of different kinds of pre-damages on the residual mechanical properties were analyzed. Results show that the stable hysteretic loops in the low-cycle fatigue tests are well-stacked. The material illustrates Masing behavior, and it has a good energy dissipation capacity. The ductility of the low-cycle fatigue-damaged materials decreases significantly in comparison with the undamaged ones. The low-cycle fatigue lives of Q345q steel are almost unaffected, so long as the pre-applied tensile strain is lower than 10%.

Keywords: plastic deformation; low-cycle fatigue; mechanical properties; pre-damage; low alloy steel; coupling damage

Citation: Liu, Q.; Tang, Z.; Yang, X.; He, Z.; Xue, H.; Zhuge, H. Mechanical Properties of Low Carbon Alloy Steel with Consideration of Prior Fatigue and Plastic Damages. *Crystals* **2022**, *12*, 967. https://doi.org/10.3390/cryst12070967

Academic Editor: Wojciech Polkowski

Received: 28 June 2022
Accepted: 7 July 2022
Published: 11 July 2022

1. Introduction

Low carbon alloy steels are widely used in the construction of buildings and bridges, energy storages such as fuel cells, and various mechanical equipment [1–3]. On the one hand, low-cycle fatigue (LCF) damage may be discovered in these structures during service due to seismic events and other extreme loading conditions. On the other hand, the materials in local regions on these steel structures and equipment may experience large plastic deformation caused by severe impact or other improper artificial operations. The coupling damage of alloy steel caused by LCF, and tensile plastic deformation is still unknown.

Fatigue of materials can be traditionally divided into high-cycle fatigue (HCF) and low-cycle fatigue scopes. Low-cycle fatigue involves bulk plasticity, whereas the deformation in high-cycle fatigue is in elastic range. A considerable number of studies on LCF of metals have been conducted to understand the fatigue life prediction and crack propagation rules [4–6]. Recently, Tsutsumi et al. [7] investigated the LCF behavior of butt-welded joints considering the inhomogeneous mechanical properties in the base metal, weld metal, and the heat-affected zones. They found that the effects of inhomogeneous material properties are very significant when evaluating the LCF of welded joints. Procházka et al. [8] studied the development of advanced techniques of the LCF test using miniature test samples. They reported that cyclic-strain and strain-life curves of the mini-sample geometries are almost of the same shape for rotor steels. Ho et al. [9] studied the LCF performance of gradient structured 316 austenitic steels under high strain amplitude loading conditions. They found that gradient structured steels exhibit inherently lower fatigue life than their

coarse-grained counterparts. Huang et al. [10] conducted monotonic tensile and ultra-low-cycle-fatigue tests on Q235 and Q690 steels to investigate the fracture behavior under various loading conditions. It was found that the deformability of Q690 steel under monotonic loading and the fatigue life under LCF loading are lower than those of Q235 steel. Tong et al. [11] evaluated the LCF life of buckling-restrained braces (BRBs), and they proposed an evaluation method for BRBs based on the combination of the cumulative plastic deformation curves. Yoon et al. [12] studied the effect of multiple high-density pulsed electric currents on the LCF life of austenitic stainless steel. An improved LCF life in austenitic stainless steel was proposed and examined by the test results. Hua et al. [13] experimentally investigated the LCF behaviors of high strength steel Q690 exposed to different elevated temperatures. A fatigue model considering the elevated temperatures was proposed to describe the relation between the total strain amplitude and the load cycles to failure. Tang et al. [14] studied the effect of structural parameters on the LCF damage evolution of thin-walled steel bridge piers. Practical formulae to evaluate the LCF damage levels were proposed and validated by experiments. Bouazza et al. [15] conducted the LCF fragility of RC bridge piers and developed an LCF fragility curve based on the performance-based earthquake engineering methodology. These above-mentioned studies were devoted to the LCF behaviors, life prediction, and fracture models of metals. However, the coupling effects of LCF damages and other types of damages of these metals were not involved.

More than 30 years ago, Park et al. [16,17] proposed a practical damage index of concrete material and members, in which the combined effects of plastic deformation and plastic energy consumption caused by cyclic loads are considered. After that, many researchers tried to reveal the relation between the cyclic damage and the plastic deformation damage of metallic materials. Cadenas–Herrera et al. [18] studied the impact of the HCF damage on the fracture toughness parameters of aluminum alloy. They reported that the tensile static mechanical properties of the material are unaffected by the prior fatigue damage. Tang et al. [19] investigated the influence of pre-fatigue damages on the alloy steel material and steel members. It was found that the tensile mechanical properties of Q345 steel decrease significantly with consideration of the prior HCF damages. Paul et al. [20] conducted material experiments under pre-LCF, followed by tensile load conditions, to study the mechanical behavior and damage evolution during cyclic plastic deformation. It was found that the pre-ratcheting has a massive effect on the subsequent LCF life. López et al. [21] studied the effect of preceding cyclic loading on the tensile behavior of titanium alloy and found that pre-damage only affects the surface of the material, but not the fundamental mechanical properties. Moćko et al. [22] investigated the change of the strain distribution on the surface of the material caused by the pre-fatigue damages using the digital image correlation method. It was found that the pre-fatigue loads can change the formation of micro-damages in the material. Tang et al. [23] experimentally studied the combined effect of HCF and LCF damages and reported that the coupling effect of different types of damages is very significant, e.g., the residual life reducing to 0.6 of the original LCF life when the prior HCF damage reaches 0.4. Wang et al. [24] investigated the influence of pre-fatigue damage on the residual mechanical properties of P92 steel. It was found that the ultimate stress of the material considering pre-fatigue shows two stages; the first one is the initial rapid degradation stage and the second one is the linear decreasing stage. Jia et al. [25] studied the LCF and extreme LCF performance of the high strength steel Q690E, and an effective constitutive model was proposed. Based on the framework of damage mechanics, Peng et al. [26] investigated the effect of average strain on the LCF life of materials under different strain cycle ratios. The relationship between the maximum strain, strain amplitude, material properties, and LCF life of the material was discussed. The above-mentioned research mainly concentrated on the effect of prior HCF/LCF damages on the tensile properties of different kinds of metals. However, the change of the mechanical behavior is very much related to the material itself. Addition-

ally, few studies have been conducted on the effect of tensile plastic deformation on the subsequent LCF behaviors.

In this research, strain-controlled fatigue tests were conducted under six different load amplitudes to study the LCF behavior of the alloy steel Q345q. Effects of the prior LCF damage on the remaining tensile properties were experimentally investigated. Moreover, the effects of the damage caused by tensile plastic deformation on the LCF behavior of the material were studied. Finally, predictive equations were proposed to determine the residual mechanical properties of the material.

2. Experimental Methods

The as-received material is low carbon alloy steel grade Q345q and its mechanical properties are similar to S355 and ASTM 50 steels [27]. Table 1 shows the chemical compositions in weight ratio of grade Q345q material provided by the factory of Baoshan Iron and Steel Co., Ltd. According to GB/T 228.1–2010 [28] and GB/T 15248–2008 [29], the shape and size of the test specimens were machined, as shown in Figure 1. All of the specimens were cut from the same plate with a nominal thickness of 10 mm. A total of 42 specimens were machined and tested for different purposes in this study. Four groups of specimens were prepared for the tensile test, the low-cycle fatigue test, the fatigue–tension test, and the tension–fatigue test, respectively.

Table 1. Chemical compositions of grade Q345q steel (wt%).

C	**Si**	**Mn**	**P**	**S**	**Nb**	**V**	**Ti**
≤0.18%	≤0.55%	0.9~1.70%	≤0.025%	≤0.02%	≤0.06%	≤0.08%	≤0.03%
Cr	**Ni**	**Cu**	**Mo**	**N**	**Als**	**Fe**	/
≤0.08%	≤0.50%	≤0.55%	≤0.20%	≤0.012%	≥0.015%	Balance	/

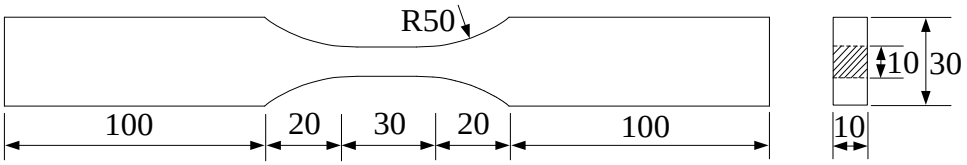

Figure 1. Geometric dimensions of specimens (mm).

Figure 2 shows the test machine with an installed specimen. The low-cycle fatigue test and the tensile test were performed on an INSTRON 8802 servo hydraulic machine in ambient air at room temperature. For the local deformation measurement, a clip-on extensometer with a gauge length of 25 mm was used and attached to the test specimens. The quasi-static tensile test was performed with a constant strain rate of 1 mm/min, while the cyclic load frequency for the low-cycle fatigue testing was kept to around 0.03 Hz. The low-cycle fatigue tests were conducted under fully reversed axial push and pull strain-controlled conditions. The test programs were designed as follows:

1. Tensile tests: to obtain the basic mechanical properties of the material such as the elastic modulus E_0, the yield stress σ_y, the ultimate stress σ_u, and the elongation at breakage δ_0. Static tensile tests were performed using 3 specimens.
2. Fatigue tests: to investigate the LCF behavior of the damage free material, a group of specimens were cyclically loaded up to fracture at selected strain amplitudes. The strain amplitude ($\Delta\varepsilon/2$) in the pure fatigue tests ranged from 1.0% to 3.0%. 18 specimens were used in the fatigue tests. The strain ratio $R = \varepsilon_{max}/\varepsilon_{min}$ was set as -1 for all fatigue load cases.
3. Tension–fatigue tests: to study the effect of large tensile plastic strain on the low-cycle fatigue behavior of the material, post-tension fatigue tests were carried out. First, the specimens were loaded with a very large deformation into the plastic stage. Afterwards, low-cycle fatigue loads were applied to the pre-damaged specimens.

9 specimens were used in the tension–fatigue tests. Triangular waveform was adopted for all cyclic loads.

4. Fatigue–tension tests: to study the effect of LCF damage on the tensile behavior of the material, pre-cyclic tests were performed to produce LCF damaged samples, and subsequent static tensile tests were carried out on these pre-damaged specimens. 12 specimens were used in these tests.

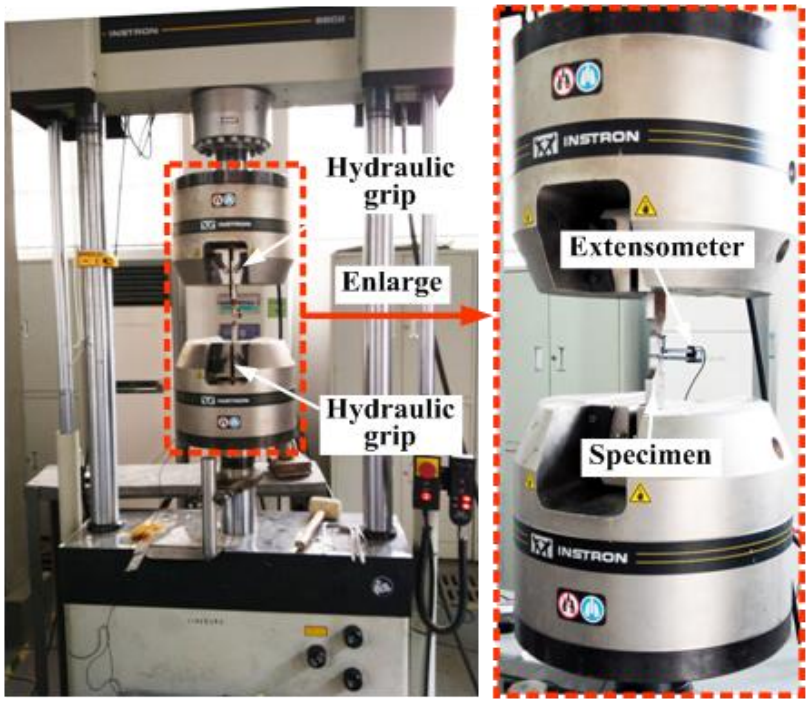

Figure 2. Test setup and instrumentation.

3. Results and Discussions

3.1. Tensile Tests

Three specimens were used in the monotonic tensile tests, in which two of them were used for repeated tests. The key parameters were derived from the stress–strain curves. Table 2 shows the monotonic tensile properties of the material, in which σ_y represent the yield stress, σ_u represents the ultimate stress, ε_u represents the ultimate strain corresponding to the ultimate stress, E_0 is the elastic modulus, and δ_0 denotes the elongation at breakage.

Table 2. Monotonic tensile properties of Q345 steel.

σ_y (MPa)	σ_u (MPa)	ε_u (%)	E_0 (GPa)	δ_0 (%)
389.6	529.2	26.0	204.2	39.5

3.2. Fatigue Tests

Constant-amplitude protocols were used for the LCF tests according to GBT 15248-2008 [29]. Six strain amplitude levels were designed, e.g., 1.0%, 1.5%, 1.7%, 2.0%, 2.5%, and 3.0%. 18 specimens were used in these tests. Figure 3 shows the hysteretic loops with different strain amplitudes in the fatigue tests. Table 3 lists the low-cycle fatigue lives of the specimens under different amplitudes of cyclic loads, in which N_f represents the fatigue life. As can be seen, low-cycle fatigue life decreases as the load amplitude increases in the constant-amplitude loading conditions.

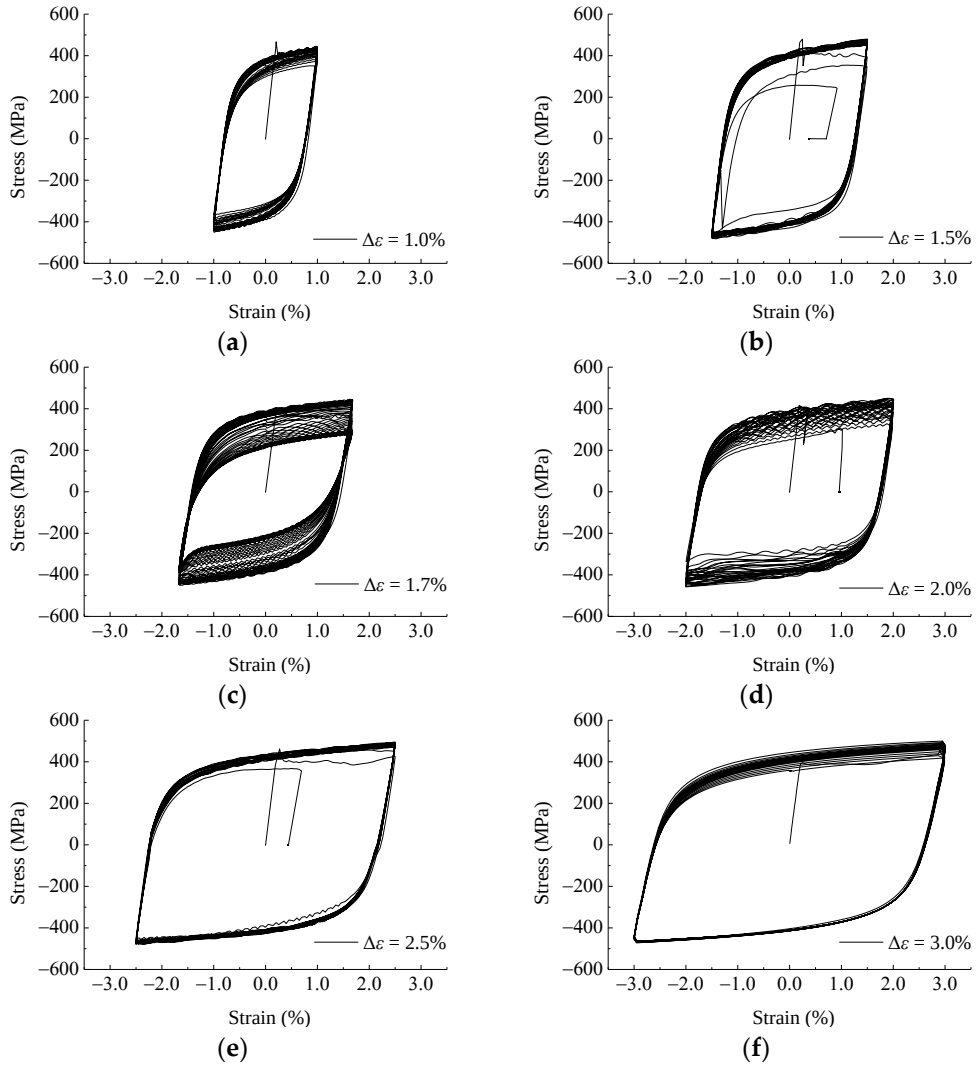

Figure 3. Hysteretic loops of low-cycle fatigue tests with strain amplitudes of: (**a**) 1.0%; (**b**) 1.5%; (**c**) 1.7%; (**d**) 2.0%; (**e**) 2.5%; (**f**) 3.0%.

Table 3. Low-cycle fatigue lives of Q345 steel.

No.	Δε/2 (%)	N_f	Average Life
1	1.0	364	405.0
2		430	
3		421	
4	1.5	276	304.7
5		312	
6		326	
7	1.7	244	234.0
8		220	
9		238	
10	2.0	214	194.7
11		198	
12		172	
13	2.5	128	139.0
14		140	
15		149	
16	3.0	71	77.7
17		65	
18		97	

The total strain amplitude in LCF tests is composed of the elastic strain amplitude component and the plastic component as such:

$$\Delta\varepsilon/2 = \Delta\varepsilon_e/2 + \Delta\varepsilon_p/2 \quad (1)$$

where $\Delta\varepsilon_e/2$ is the elastic strain amplitude part, and $\Delta\varepsilon_p/2$ is the plastic strain amplitude part.

The relation between the LCF lives and the plastic strain amplitudes can be described by the Coffin–Manson equation:

$$\Delta\varepsilon_p/2 = \varepsilon'_f \cdot (2N_f)^c \quad (2)$$

where ε'_f is the fatigue ductility coefficient and c is the fatigue ductility exponent.

Figure 4 shows the fatigue lives of the test specimens and the fitting strain–fatigue life relation (see Equation (3)), which can be used to predict the LCF life of this kind of steel material.

$$\Delta\varepsilon_p/2 = 0.843 \cdot (2N_f)^{-0.64} \quad (3)$$

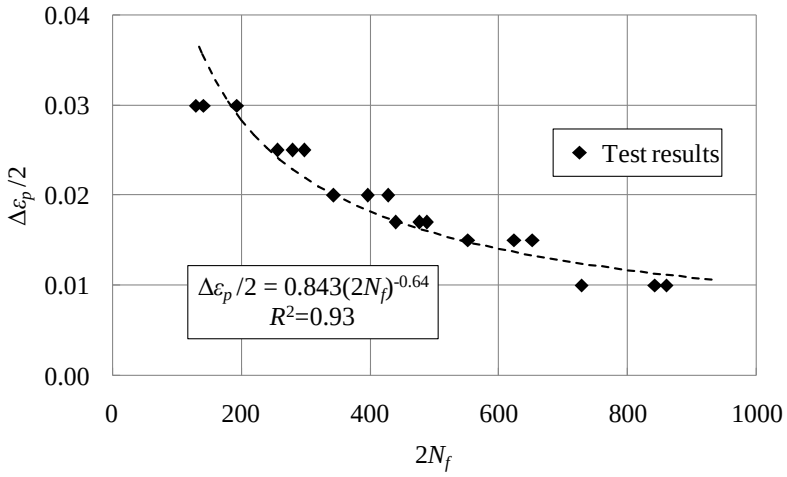

Figure 4. Fitting results based on the LCF tests.

Figure 5 shows the stress–strain loops at the $N_f/2$ load cycle under different strain amplitude conditions. It can be seen that the maximum stress in each case is basically on the coincident curves, and all the hysteretic loops are well-stacked and in a stable state. This means this kind of steel material illustrates Masing behavior, and it has a good energy dissipation capacity. Hysteretic curves can be fitted using the Ramberg–Osgood equation [30], and for LCF tests, the relation between the cyclic stress and strain can be expressed as:

$$\Delta\sigma/2 = K' \cdot (\Delta\varepsilon_p/2)^{n'} \quad (4)$$

where $\Delta\sigma/2$ is the stable stress amplitude, K' is the cyclic hardening coefficient, and n' is the cyclic hardening index. These stable values are obtained from the stress–strain loops at the $N_f/2$ load cycle as shown in Figure 5. The parameters in the Ramberg–Osgood equation can be calibrated via these experimental results. Parameter K' is 395.8 and n' is 0.118 for the low alloy steel Q345.

3.3. Fatigue-Tension Tests

The fatigue–tension tests were conducted to investigate the remaining mechanical properties of the specimens after being fatigue damaged. A constant strain amplitude of 1.7% was adopted in the fatigue–tension tests. Therefore, the corresponding fatigue life at this strain amplitude is 234.0 according to the previous pure fatigue tests. Eight different pre-fatigue levels were selected by applying different numbers of load loops (10, 20, 30, 40, 50, 60, 70, and 200) to the specimens. The pre-damage levels are represented using the

ratio of the applied load cycles N and the corresponding fatigue life N_f. Figure 6 shows the stress–strain curves of the fatigue–tension tests, in which the static tensile curves are also illustrated for comparison. As can be seen, the ductility of the fatigue-damaged specimens decreases dramatically. When the specimen is severely fatigue-damaged, e.g., $N/N_f = 0.855$, both the strength and ductility degrade significantly.

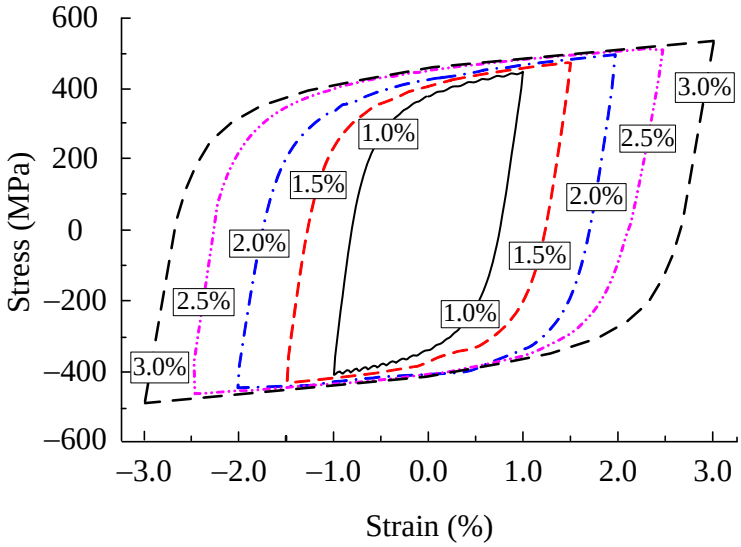

Figure 5. Stabilized cyclic stress–strain hysteretic loops in low-cycle fatigue tests.

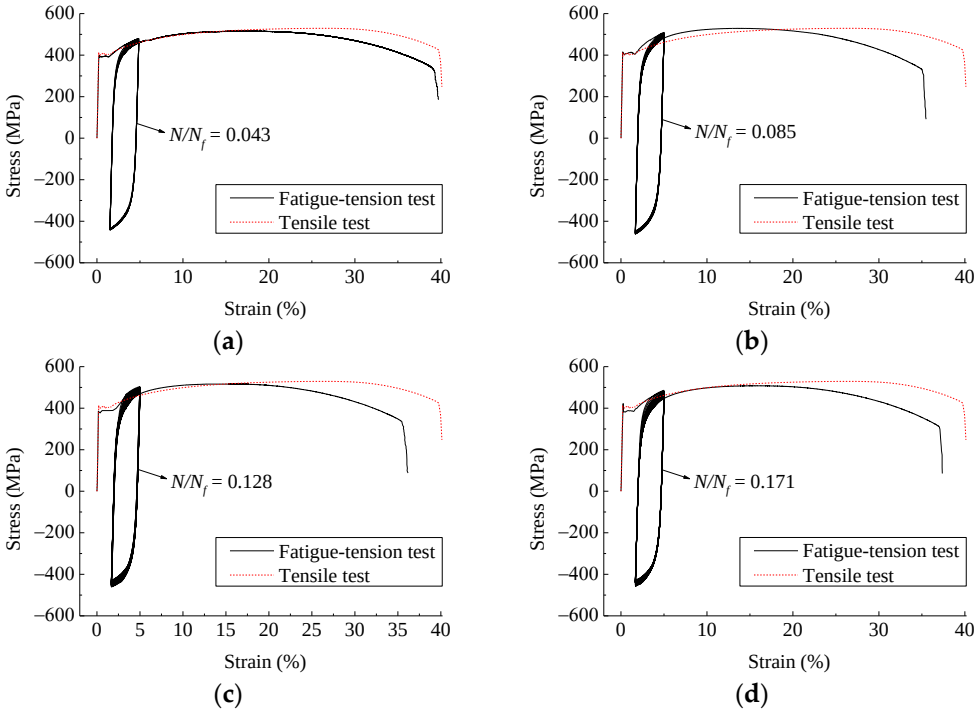

Figure 6. *Cont.*

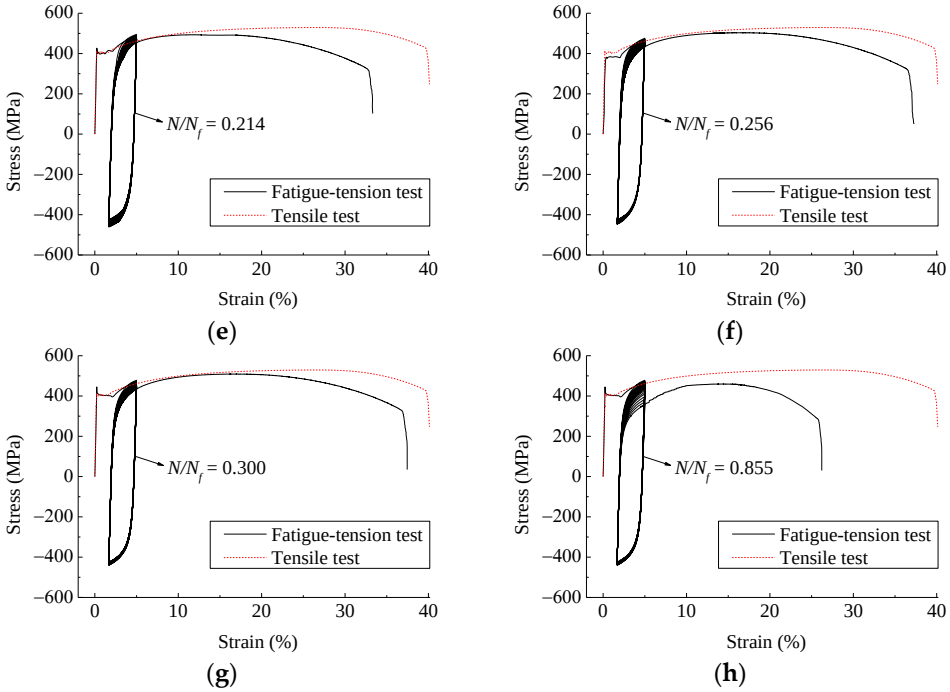

Figure 6. The stress–strain curves of fatigue-tension tests with strain amplitude of 1.70% and pre-fatigue damages of: (**a**) 0.043; (**b**) 0.085; (**c**) 0.128; (**d**) 0.171; (**e**) 0.214; (**f**) 0.256; (**g**) 0.300; (**h**) 0.855.

The fatigue–tension tests were also conducted with a constant strain amplitude of 2.5% to study the effects of the load amplitudes. The corresponding fatigue life with a strain amplitude of 2.5% is 139.0. Four different pre-fatigue levels were designed by applying 10, 20, 30, and 40 load cycles to the specimens. Figure 7 shows the stress–strain curves of the fatigue–tension tests with strain amplitude of 2.5%. As can be seen, the ultimate stress is almost unaffected by the pre-fatigue damage in these cases.

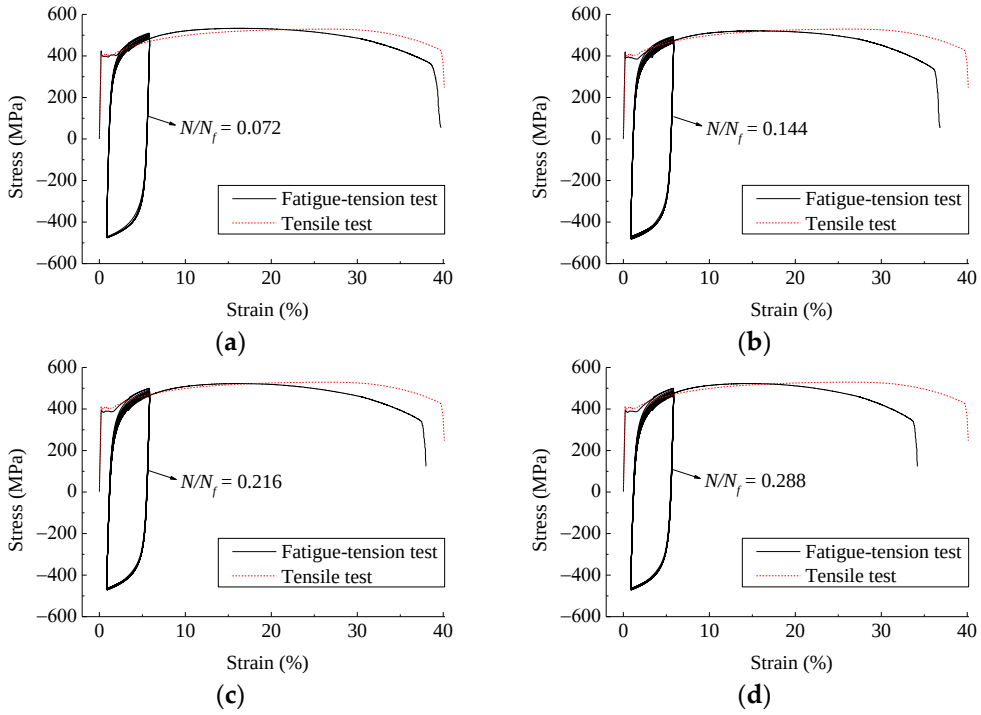

Figure 7. The stress–strain curves of fatigue–tension tests with a strain amplitude of 2.5% and pre-fatigue damages of: (**a**) 0.072; (**b**) 0.144; (**c**) 0.216; (**d**) 0.288.

Figure 8 shows the remaining mechanical properties of the specimens after being fatigue damaged, in which σ'_u represents the remaining ultimate stress, ε'_u represents the ultimate strain corresponding to the remaining ultimate stress, and δ denotes the elongation of the specimens with pre-fatigue damages. As can be seen in the figure, the ultimate strength and the elongation decrease as the pre-fatigue damages increase. The strain amplitudes of the cyclic loads have no significant effects on the deterioration tendency of the mechanical properties. Notable among the deterioration of the mechanical properties, the ultimate strain ε'_u corresponding to the ultimate stress decreases remarkably even if the pre-fatigue damage is slight, which indicates an earlier decrease of the tensile stress–strain curves (see Figures 6 and 7). The fitting equations of the test results are also given in these figures (see Equations (5)–(7)), which can be adopted for the prediction of the remaining mechanical properties of the fatigue-damaged materials. Note that for the fitting of the test results ε'_u, the result of the undamaged specimen was not used (Figure 8b).

$$\sigma'_u/\sigma_u = -0.151\cdot(N/N_f) + 1.000 \quad (5)$$

$$\varepsilon'_u/\varepsilon_u = -0.114\cdot(N/N_f) + 0.627 \quad (6)$$

$$\delta'_u/\delta_0 = -0.372\cdot(N/N_f) + 0.974 \quad (7)$$

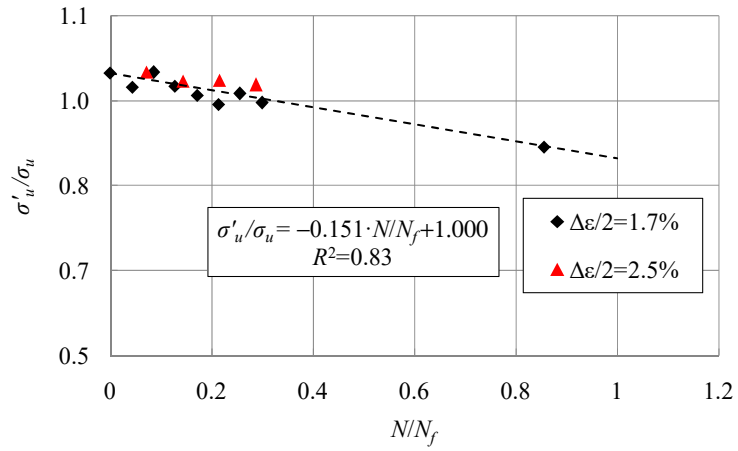

(**a**)

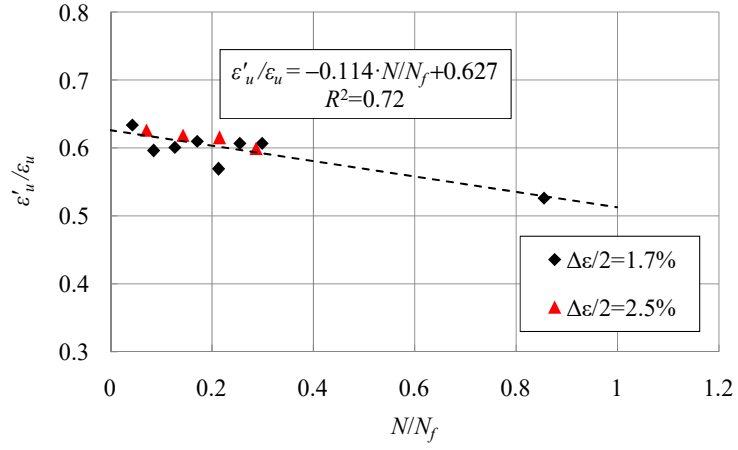

(**b**)

Figure 8. *Cont.*

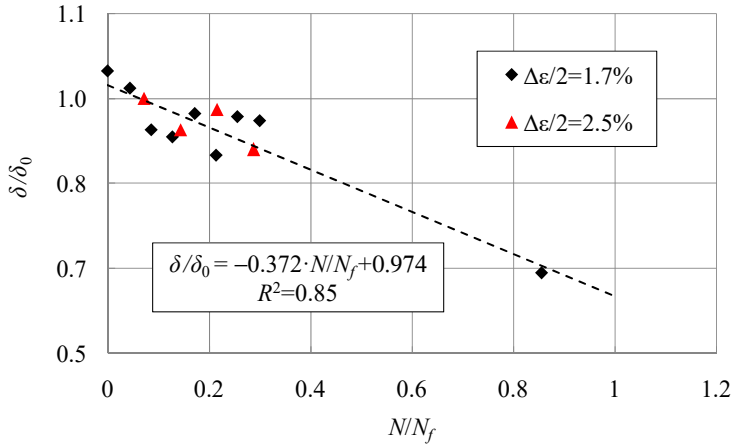

(**c**)

Figure 8. The remaining mechanical properties of the specimens after being fatigue damaged; (**a**) remaining ultimate stress; (**b**) strain corresponding to remaining ultimate stress; (**c**) remaining elongation at breakage.

3.4. Tension-Fatigue Tests

In this section, the effects of pre-damages caused by a large tensile plastic deformation on the LCF behavior of the low alloy steel are studied. Consequently, the tension–fatigue tests were performed, in which the specimens were firstly subjected to tensile strains of 3.35%, 4.20%, 5.03%, 5.86%, 6.70%, 7.54%, 8.38%, 9.20, and 10.10% to generate different pre-damage levels, and then subsequent low-cycle fatigue loads were applied to the same specimens. Figure 9 shows the stress–strain curves obtained from the tension–fatigue tests, in which constant strain amplitude of 1.7% was selected. Table 4 shows the remaining LCF lives of the specimens with consideration of the pre-damages caused by prior tensile deformation, in which N'_f represents the remaining fatigue life.

Table 4. Test results of the tension–fatigue tests.

No.	ε_t (%)	N'_f
1	3.35	185
2	4.20	221
3	5.03	192
4	5.86	180
5	6.70	190
6	7.54	247
7	8.38	201
8	9.20	229
9	10.10	238

Figure 10 shows the remaining LCF lives of the pre-damaged specimens, in which the fatigue life of the specimen without pre-damage is also indicated. As can be seen, the fatigue lives decrease due to the pre-damages induced by the tensile deformation in most cases. However, this kind of effect is not so notable. The remaining fatigue lives of the specimens with previous tensile deformation damages of 7.54% and 10.10% are even longer than that of the undamaged ones. Considering the large dispersion of the fatigue test results, it can be concluded that the fatigue lives are almost unaffected as long as the pre-applied tensile strain is lower than 10%.

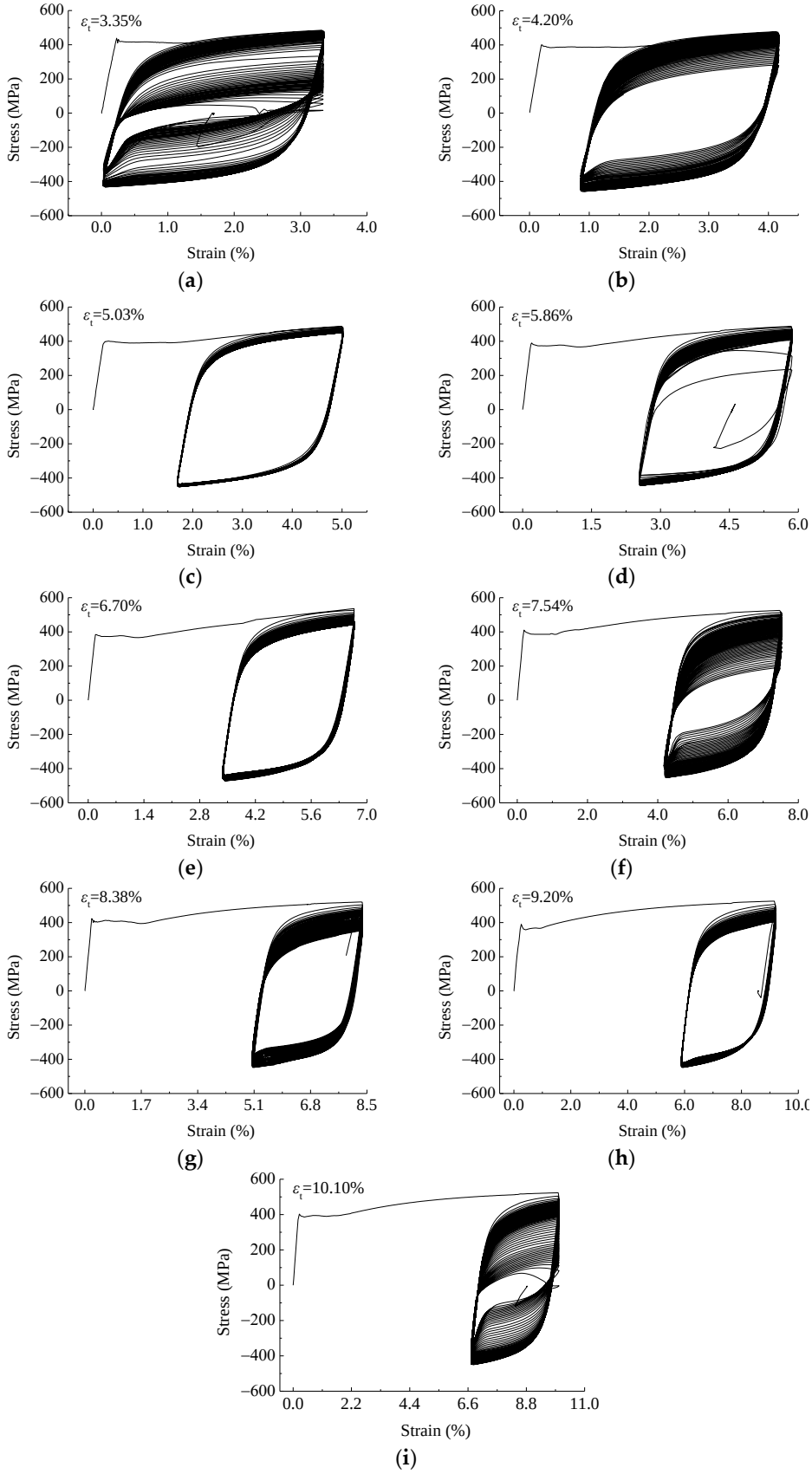

Figure 9. The stress–strain curves of tension–fatigue tests with a prior maximum tensile strain of: (**a**) 3.35%; (**b**) 4.20%; (**c**) 5.03%; (**d**) 5.86%; (**e**) 6.70%; (**f**) 7.54%; (**g**) 8.38%; (**h**) 9.20%; (**i**) 10.10%.

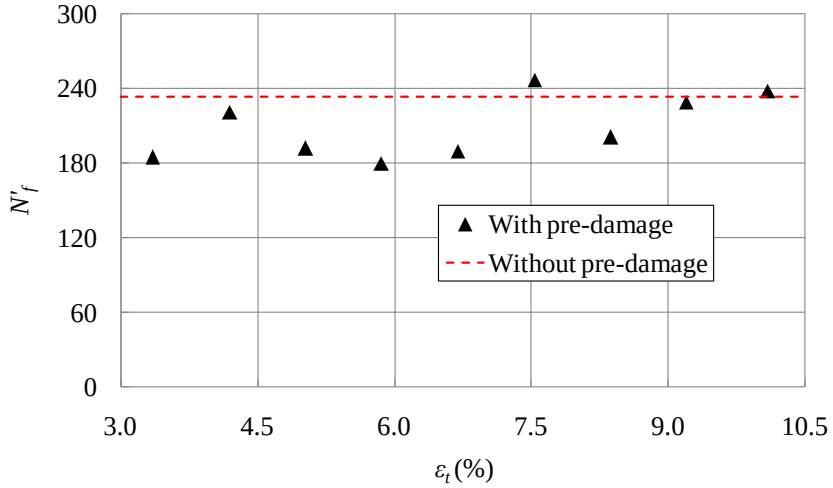

Figure 10. The remaining low-cycle fatigue lives considering prior tensile deformation damages.

4. Conclusions

The low-cycle fatigue behavior, the remaining mechanical properties with consideration of low-cycle fatigue damages, and the remaining fatigue lives considering the prior plastic deformation damages of low carbon alloy steel Q345q were experimentally studied herein. The following conclusions can be drawn, and they are limited to Q345q steel, which was adopted in the tests of this study.

1. The Manson–Coffin formula of Q345q steel was obtained based on the pure fatigue tests, which can be used to predict the low-cycle fatigue life of this kind of material. The stable hysteretic loops are well-stacked. The material illustrates Masing behavior, and it has a good energy dissipation capacity.
2. The ductility of the LCF-damaged materials decreases in comparison with the undamaged ones. When the specimen is severely fatigue-damaged, e.g., $N/N_f = 0.855$, both the strength and the ductility degrade significantly.
3. The strain amplitudes of the prior cyclic loads have no significant effects on the deterioration tendency of the remaining mechanical properties. The strain corresponding to the ultimate stress decreases remarkably, indicating an earlier decrease of the tensile stress–strain curves.
4. The obtained fitting equations of the remaining mechanical properties of the fatigue-damaged specimens can be adopted for the plastic behavior prediction of the LCF-damaged steel materials.
5. The low-cycle fatigue lives of Q345q steel are almost unaffected, as long as the pre-applied tensile strain is lower than 10%.

Author Contributions: Conceptualization, Z.T. and Z.H.; methodology, Z.T.; software, Q.L.; validation, Z.T. and Q.L.; formal analysis, Q.L. and X.Y.; investigation, H.X.; resources, Z.T.; data curation, Q.L. and Z.T.; writing—original draft preparation, Z.T. and Q.L.; writing—review and editing, Z.H. and H.Z.; visualization, Q.L.; supervision, Z.T.; project administration, Z.T.; funding acquisition, Z.T. All authors have read and agreed to the published version of the manuscript.

Funding: This research was funded by the Postgraduate Research & Practice Innovation Program of Jiangsu Province (SJCX22_1747, KYCX21_3225), the Qing Lan Project of Yangzhou University, and the National Natural Science Foundation of China (51708485).

Institutional Review Board Statement: Not applicable.

Informed Consent Statement: Not applicable.

Data Availability Statement: Data is contained within the article.

Acknowledgments: The corresponding author gratefully acknowledges the support of Yangzhou Zhongde Mining Machinery Co., LTD., Yangzhou, China for the manufacturing and testing work of some of the specimens.

Conflicts of Interest: The authors declare no conflict of interest.

References

1. Smith, B.H.; Szyniszewski, S.; Hajjar, J.F.; Schafer, B.W.; Arwade, S.R. Steel foam for structures: A review of applications, manufacturing and material properties. *J. Constr. Steel Res.* **2012**, *71*, 1–10. [CrossRef]
2. Stornelli, G.; Gaggiotti, M.; Mancini, S.; Napoli, G.; Rocchi, C.; Tirasso, C.; Di Schino, A. Recrystallization and grain growth of AISI 904L super-austenitic stainless steel: A multivariate regression approach. *Metals* **2022**, *12*, 200. [CrossRef]
3. Di Schino, A. Analysis of phase transformation in high strength low alloyed steels. *Metalurgija* **2017**, *56*, 349–352.
4. Guo, Y.; Fang, C.; Zheng, Y. Post-fire hysteretic and low-cycle fatigue behaviors of Q345 carbon steel. *J. Constr. Steel Res.* **2021**, *187*, 106991. [CrossRef]
5. Dong, Q.; Yang, P.; Xu, G.; Deng, J. Mechanisms and modeling of low cycle fatigue crack propagation in a pressure vessel steel Q345. *Int. J. Fatigue* **2016**, *89*, 2–10. [CrossRef]
6. Liao, F.; Wang, W.; Chen, Y. Parameter calibrations and application of micromechanical fracture models of structural steels. *Struct. Eng. Mech.* **2012**, *42*, 153–174. [CrossRef]
7. Tsutsumi, S.; Fincato, R.; Luo, P.; Sano, M.; Umeda, T.; Kinoshita, T.; Tagawa, T. Effects of weld geometry and HAZ property on low-cycle fatigue behavior of welded joint. *Int. J. Fatigue* **2022**, *156*, 106683. [CrossRef]
8. Procházka, R.; Džugan, J. Low cycle fatigue properties assessment for rotor steels with the use of miniaturized specimens. *Int. J. Fatigue* **2022**, *154*, 106555. [CrossRef]
9. Ho, H.S.; Lv, C.; Zhou, W.; Zhang, E. Low-cycle fatigue behavior of gradient structured austenitic stainless steels under high strain amplitude. *Fatigue Fract. Eng. Mater. Struct.* **2022**, *45*, 1818–1829. [CrossRef]
10. Huang, X.; Yuan, Y.; Zhao, J.; Wei, C. Comparative study on ultra-low-cycle-fatigue behavior of Q235 normal-steel and Q690 high-strength steel. *J. Constr. Steel Res.* **2022**, *194*, 107308. [CrossRef]
11. Tong, C.; Wu, J.; Hua, K.; Tian, H. Low-cycle fatigue life evaluation of buckling-restrained braces based on cumulative plastic deformation curves. *Adv. Struct. Eng.* **2022**, *25*, 336–354. [CrossRef]
12. Yoon, S.; Cui, Y.; Kimura, Y.; Gu, S.; Toku, Y.; Ju, Y. Improvement of low-cycle fatigue life of austenitic stainless steel by multiple high-density pulsed electric currents. *Int. J. Fatigue* **2022**, *156*, 106639. [CrossRef]
13. Hua, J.; Yang, Z.; Zhou, F.; Hai, L.; Wang, N.; Wang, F. Effects of exposure temperature on low–cycle fatigue properties of Q690 high–strength steel. *J. Constr. Steel Res.* **2022**, *190*, 107159. [CrossRef]
14. Tang, Z.Z.; Xue, H.Y.; Liu, H.; Zhang, W. Prediction of ultralow cycle fatigue damage of thin-walled steel bridge piers. *Adv. Steel Constr.* **2021**, *17*, 403–411.
15. Bouazza, H.; Djelil, M.; Matallah, M. On the relevance of incorporating bar slip, bar buckling and low-cycle fatigue effects in seismic fragility assessment of RC bridge piers. *Eng. Struct.* **2022**, *256*, 114032. [CrossRef]
16. Park, Y.J.; Ang, A.H. Mechanistic seismic damage model for reinforced concrete. *J. Struct. Eng.* **1985**, *111*, 722–739. [CrossRef]
17. Park, Y.J.; Ang, A.H.; Wen, Y.K. Damage-limiting aseismic design of buildings. *Earthq. Spectra* **1987**, *3*, 1–26. [CrossRef]
18. Cadenas-Herrera, P.; Amrouche, A.; Mesmacque, G.; Jozwiak, K.; Puchi-cabrera, E.S. Influence of residual fatigue damage on the fracture toughness parameters of an AA6082-T6 aluminium alloy. *Fatigue Fract. Eng. Mater. Struct.* **2010**, *33*, 54–65. [CrossRef]
19. Tang, Z.; Hu, X.; Jiang, J.; Xue, H.; Zhuge, H. Effects of pre-fatigue damages on ultimate strength of steel columns: From material to structure. *J. Constr. Steel Res.* **2022**, *195*, 107358. [CrossRef]
20. Paul, S.K.; Sivaprasad, S.; Dhar, S.; Tarafder, S. Cyclic plastic deformation and damage in 304LN stainless steel. *Mater. Sci. Eng. A* **2011**, *528*, 4873–4882. [CrossRef]
21. López, J.G.; Verleysen, P.; Baere, I.D.; Degrieck, J. Tensile properties of thin-sheet metals after cyclic damage. *Procedia Eng.* **2011**, *10*, 1961–1966. [CrossRef]
22. Moćko, W.; Brodecki, A.; Radziejewska, J. Effects of pre-fatigue on the strain localization during tensile test s of DP500 steel at low and high strain rates. *J. Strain Anal. Eng. Des.* **2015**, *50*, 349–351. [CrossRef]
23. Tang, Z.; Chen, Z.; He, Z.; Hu, X.; Xue, H.; Zhuge, H. Experimental and numerical study of combined high and low cycle fatigue performance of low alloy steel and engineering application. *Materials* **2021**, *14*, 3395. [CrossRef] [PubMed]
24. Wang, X.; Zhang, W.; Ni, J.; Zhang, T.; Gong, J.; Wahab, M.A. Quantitative description between pre-fatigue damage and residual tensile properties of P92 steel. *Mater. Sci. Eng. A* **2019**, *744*, 415–425. [CrossRef]
25. Jia, C.; Shao, Y.; Guo, L.; Liu, H. Cyclic behavior and constitutive model of high strength low alloy steel plate. *Eng. Struct.* **2020**, *217*, 110798. [CrossRef]
26. Peng, Y.; Liu, Y.; Li, H.; Xing, J. Research on low cycle fatigue life prediction considering average strain. *Mater. Res. Express* **2022**, *9*, 016521. [CrossRef]
27. *GB/T 714–2015*; General Administration of Quality Supervision, Inspection and Quarantine of the People's Republic of China, Structural Steel for Bridge. Standards Press of China: Beijing, China, 2015.

28. *GB/T 228.1–2010*; General Administration of Quality Supervision, Inspection and Quarantine of China, Metallic Materials-Tensile Testing-Part1: Methods of Test at Room Temperature. Standards Press of China: Beijing, China, 2011.
29. *GB/T 15248–2008*; General Administration of Quality Supervision, Inspection and Quarantine of China, The Test Method for Axial Loading Constant-Amplitude Low-Cycle Fatigue of Metallic Materials. Standards Press of China: Beijing, China, 2011.
30. Ramberg, W.; Osgood, W.R. Description of Stress-Strain Curves by Three Parameters. 1943. Available online: https://ntrs.nasa.gov/citations/19930081614 (accessed on 8 July 2022).